

Ergodic theory, Dynamic Mode Decomposition and Computation of Spectral Properties of the Koopman operator

Hassan Arbabi¹ and Igor Mezić^{2*}

January 3, 2023

Abstract

Dynamic Mode Decomposition (DMD) is a class of numerical algorithms for computation of the eigenvalues and eigenfunctions of the Koopman operator. In this paper, we establish the convergence of a class of such algorithms to eigenvalues and eigenfunctions of the infinite-dimensional Koopman operator. The algorithms act on data coming from observables on a state space, arranged in Hankel-type matrices. The proofs utilize the assumption that the underlying dynamical system is ergodic. This includes the classical measure-preserving systems, as well as systems whose attractors support a physical measure. Our approach relies on the observation that vector projections in DMD can be used to approximate the function projections by the virtue of Birkhoff's ergodic theorem. Using this fact, we show that applying DMD to Hankel data matrices in the limit of infinite-time observations yields the true Koopman eigenfunctions and eigenvalues. We also show that the Singular Value Decomposition, which is the central part of most DMD algorithms, converges to the Proper Orthogonal Decomposition of observables. We use this result to obtain a representation of the dynamics of systems with continuous spectrum. The numerical application of these methods is demonstrated using examples from well-known dynamical systems and computational fluid dynamics.

Keywords: Koopman operator, Ergodic theory, Dynamic Mode Decomposition (DMD), Hankel matrix, Singular Value Decomposition (SVD), Proper Orthogonal Decomposition (POD)

1 INTRODUCTION

The Koopman operator framework has proved useful in study of high-dimensional dynamical systems. This point of view in dynamical system is originated in 1930's through the work of Bernard Koopman and John Von Neumann ([1, 2]). In particular, Koopman realized that the evolution of observables on the state space of a Hamiltonian system can be described via a linear transformation, which was later named the Koopman operator. The renewed interest in this formalism was sparked by [3] and [4], in which a spectral decomposition was proved that was later on supplemented by numerical algorithms allowing its use in high-dimensional dynamical systems (see e.g. [5, 6, 7, 8, 9]). In this section, we briefly review the Koopman operator theory for continuous- and discrete-time dynamical systems. The reader is referred to [10] for a more detailed exposition.

^{*1}Hassan Arbabi is with the department of Mechanical Engineering, University of California, Santa Barbara, CA, 93106, USA harbabi@engr.ucsb.edu

^{*2}Igor Mezić is with the faculty of Mechanical Engineering and Mathematics, University of California, Santa Barbara, CA, 93106, USA mezic@engr.ucsb.edu

Consider a continuous-time dynamical system given by

$$\dot{\mathbf{x}} = \mathbf{F}(\mathbf{x}), \quad (1)$$

on a state space M (i.e. $\mathbf{x} \in M$ - where we by slight abuse of notation identify a point in a manifold M with its vector representation \mathbf{x} in \mathbb{R}^m , m being the dimension of the manifold), where \mathbf{x} is a vector and \mathbf{F} is a possibly nonlinear vector-valued smooth function, of the same dimension as its argument \mathbf{x} . Let $\mathbf{S}^t(\mathbf{x}_0)$ denote the position at time t of trajectory of (1) that starts at time 0 at point \mathbf{x}_0 . We call $\mathbf{S}^t(\mathbf{x}_0)$ the flow generated by (1).

Denote by \mathbf{f} an arbitrary, vector-valued function from M to \mathbb{C}^k . We call \mathbf{f} an observable of the system in (1). The value of \mathbf{f} that is observed on a trajectory starting from \mathbf{x}_0 at time 0 changes with time according to the flow, i.e.,

$$\mathbf{f}(t, \mathbf{x}_0) = \mathbf{f}(\mathbf{S}^t(\mathbf{x}_0)). \quad (2)$$

Note that the space of all observables \mathbf{f} is a linear vector space, and we can define a family of linear operators U^t with $t \in [0, \infty)$, acting on this vector space, by

$$U^t \mathbf{f}(\mathbf{x}_0) = \mathbf{f}(\mathbf{S}^t(\mathbf{x}_0)). \quad (3)$$

Thus, for a fixed time τ , U^τ maps the vector-valued observable $\mathbf{f}(\mathbf{x}_0)$ to $\mathbf{f}(\tau, \mathbf{x}_0)$. We will call the family of operators U^t , indexed by time t , the Koopman operator of the continuous-time system (1). In operator theory, such operators defined for general dynamical systems, are often called composition operators, since U^t acts on observables by composing them with the flow \mathbf{S}^t [11].

In discrete-time the definition is even simpler, if

$$\mathbf{z}' = \mathbf{T}(\mathbf{z}), \quad (4)$$

is a discrete-time dynamical system with $\mathbf{z} \in M$, then the associated Koopman operator U is defined by

$$U\mathbf{f}(\mathbf{z}) = \mathbf{f} \circ \mathbf{T}(\mathbf{z}).$$

The operator U is linear, i.e.,

$$U(c_1 \mathbf{f}_1(\mathbf{z}) + c_2 \mathbf{f}_2(\mathbf{z})) = c_1 \mathbf{f}_1(\mathbf{T}(\mathbf{z})) + c_2 \mathbf{f}_2(\mathbf{T}(\mathbf{z})) = c_1 U\mathbf{f}_1(\mathbf{z}) + c_2 U\mathbf{f}_2(\mathbf{z}). \quad (5)$$

A similar calculation shows the linearity of the Koopman operator for a continuous-time system in (1). We call $\phi : M \rightarrow \mathbb{C}$ an eigenfunction of the Koopman operator U , associated with eigenvalue $\lambda \in \mathbb{C}$, when

$$U\phi = \lambda\phi.$$

For the continuous-time system, the definition is slightly different:

$$U^t \phi = e^{\lambda t} \phi.$$

The eigenfunctions and eigenvalues of the Koopman operator can be utilized to analyze the underlying dynamical system in (1) or (4). For example, the level sets of the eigenfunctions can be used to determine the state-space geometry [12], and the global stability of equilibria can be characterized by considering the eigenvalues and eigenfunctions of the Koopman operator [13]. Another outcome of this theory, which is specially useful for high-dimensional systems, is the Koopman mode decomposition (KMD). If the Koopman spectrum consists of only (discrete) eigenvalues, the

evolution of observables can be expanded in terms of the Koopman eigenfunctions, denoted by ϕ_j , $j = 0, 1, \dots$, and Koopman eigenvalues λ_j . Consider again the observable $\mathbf{f} : M \rightarrow \mathbb{C}^k$, then the evolution of \mathbf{f} under the discrete system in (4) is given by

$$U^n \mathbf{f}(z_0) := \mathbf{f} \circ \mathbf{T}^n(z_0) = \sum_{j=1}^{\infty} \mathbf{v}_j \phi_j(z_0) \lambda_j^n. \quad (6)$$

In the above decomposition, $\mathbf{v}_j \in \mathbb{C}^k$ is the Koopman mode associated with the pair (λ_j, ϕ_j) and is given by the projection of the observable \mathbf{g} onto the eigenfunction ϕ_j . These modes correspond to components of the physical field characterized by exponential growth and/or oscillation in time and play an important role in the analysis of large systems (see the references in the first paragraph).

In recent years a variety of methods have been developed for computation of the Koopman spectral properties (eigenvalues, eigenfunctions and modes) from data sets that describe the evolution of observables such as \mathbf{f} . A large fraction of these methods belong to the class of algorithms known as Dynamic Mode Decomposition, or DMD in short (see e.g. [5, 6, 14, 15]). In this paper, we prove that the eigenvalues and eigenfunctions obtained by DMD methods converge to the eigenvalues and eigenfunctions of the infinite-dimensional Koopman operator for ergodic systems. Such proofs—that finite-dimensional approximations of spectra converge to spectra of infinite-dimensional linear operators—are still rare and mostly done for self-adjoint operators [16] (Koopman operator is typically not self-adjoint). Our approach here provides a new - ergodic theory inspired - proof, the strategy of which could be used in other contexts of non-self adjoint operators. The outline of this paper is as follows:

In section 2, we describe the three earliest variants of DMD, namely, the companion-matrix DMD, SVD-enhanced DMD and Exact DMD. The sections 3-5 tend to the computation of the Koopman eigenvalues and eigenfunctions for ergodic system with discrete spectrum. In section 3, we review some elementary ergodic theory, and present a new variation of DMD algorithm - the Hankel-DMD method - for computation of Koopman spectrum by observations on a single observable. In section 3.2, we extend the application of this method to observations on trajectories that converge to an ergodic attractor. In section 4, we make a precise connection between the Singular Value Decomposition (SVD) on data matrices and Proper Orthogonal Decomposition (POD) on the ensemble of observables on ergodic dynamical systems. Our motivation is to give an understanding of the SVD applications, which plays a central role in DMD algorithms. In fact, by using this interpretation of SVD, we are able to show the convergence of the Exact DMD for ergodic systems in section 5. These results enable us to extract the Koopman spectral properties from measurements on multiple observables. We also present a variation of this algorithm, called Exact Hankel-DMD method, and demonstrate an application of this method by revisiting the example from the computational fluid dynamics. We summarize our results in section 6.

2 Review of Dynamic Mode Decomposition (DMD)

The three variants of DMD that we consider in this work: 1) the companion-matrix method proposed by Rowley et al. [5], 2) the SVD-enhanced DMD developed by Schmid [6], and 3) the Exact DMD method introduced by Tu et al. [14]. We also discuss the connection between these algorithms and describe the conditions, under which, they yield the same approximation of the Koopman mode decomposition. There are also other variants of DMD that we do not discuss in this work (see e.g. [15] and [17]).

Let

$$\mathbf{f} := \begin{bmatrix} f_1 \\ f_2 \\ \vdots \\ f_n \end{bmatrix} : M \rightarrow \mathbb{R}^n \quad (7)$$

be a vector-valued observable defined on the dynamical system defined in (4), and let

$$D := \begin{bmatrix} f_1(z_0) & f_1 \circ T(z_0) & \dots & f_1 \circ T^m(z_0) \\ f_2(z_0) & f_2 \circ T(z_0) & \dots & f_2 \circ T^m(z_0) \\ \vdots & \vdots & \ddots & \vdots \\ f_n(z_0) & f_n \circ T(z_0) & \dots & f_n \circ T^m(z_0) \end{bmatrix} \quad (8)$$

the matrix of measurements recorded on \mathbf{f} along a trajectory starting at the initial condition $z_0 \in M$. Each column of D is called a *data snapshot* since it holds the measurements on the system at a single time instant. Assuming only discrete eigenvalues for the Koopman operator, we can rewrite the Koopman mode expansion in (6) for the snapshots in the form of

$$D_i := \begin{bmatrix} f_1 \circ T^i(z_0) \\ f_2 \circ T^i(z_0) \\ \vdots \\ f_n \circ T^i(z_0) \end{bmatrix} = \sum_{j=1}^{\infty} \lambda_j^i \mathbf{v}_j \quad (9)$$

by absorbing the scalar values of $\phi_j(z_0)$ into the mode \mathbf{v}_j . In numerical approximation of the Koopman modes, however, we often assume this expansion is finite dimensional and use

$$\mathbf{f}^i = \sum_{j=1}^n \tilde{\lambda}_j^i \tilde{\mathbf{v}}_j \quad (10)$$

where $\tilde{\mathbf{v}}_j$ and $\tilde{\lambda}_j$ are approximations to the Koopman modes and eigenvalues in (9). This finite-dimensional expansion matches the spectral expansion for a linear operator acting on \mathbb{R}^n . This operator, which maps each column of D to the next is called the *DMD operator*. The general strategy of DMD algorithms ([5, 6, 14]) is to construct the DMD operator, in the form of a matrix, and extract the dynamic modes and eigenvalues from the spectrum of that matrix. First, we present the companion-matrix DMD algorithm introduced by [5]. In this method, as the name suggests, the DMD operator is realized in the form of a companion matrix.

Algorithm 1 (Companion-matrix DMD). Consider the data matrix D defined in (8).

1. Define $X = [D_0 \ D_1 \ \dots \ D_{m-1}]$.
2. Form the companion matrix

$$\tilde{C} = \begin{pmatrix} 0 & 0 & \dots & 0 & \tilde{c}_0 \\ 1 & 0 & \dots & 0 & \tilde{c}_1 \\ 0 & 1 & \dots & 0 & \tilde{c}_2 \\ \vdots & \vdots & \ddots & \vdots & \vdots \\ 0 & 0 & \dots & 1 & \tilde{c}_{m-1} \end{pmatrix}, \quad (11)$$

with

$$(c_0, c_1, c_2, \dots, c_{m-2})^T = X^\dagger D_m.$$

The X^\dagger denotes the Moore-Penrose pseudo-inverse of X [18].

3. Let (λ_j, w_j) , $j = 1, 2, \dots, m$ be the eigenvalue-eigenvector pairs for \tilde{C} . Then λ_j 's are the dynamic eigenvalues. Dynamic modes \tilde{v}_j are given by

$$\tilde{v}_j = X w_j, \quad j = 1, 2, \dots, m. \quad (12)$$

In the above algorithm the companion matrix \tilde{C} , is the realization of the DMD operator in the basis which consists of the columns in X . The pseudo-inverse in step 2 is used to project the last snapshot of D onto this basis. In case that D_m lies in the range of X , we have

$$r := D_m - X(X^\dagger D_m) = 0 \quad (13)$$

which means that the companion matrix \tilde{C} exactly maps each column of D to the next. If columns of X are linearly dependent, however, the above projection is not unique, and the problem of determining the DMD operator is generally over-constrained. Furthermore, in numerical practice, when X is ill-conditioned, the projection in step 2 becomes numerically unstable. The SVD-enhanced DMD algorithm, introduced by Schmid [6], offers a more robust algorithm for computation of dynamic modes and eigenvalues.

Algorithm 2 (SVD-enhanced DMD). Consider the data matrix D defined in (8).

1. Define $X = [D_0 \ D_1 \ \dots \ D_{m-1}]$ and $Y = [D_1 \ D_2 \ \dots \ D_m]$.
2. Compute the SVD of X :

$$X = W S \tilde{V}^*. \quad (14)$$

3. Form the matrix

$$\hat{A} = W^* Y \tilde{V} S^{-1}. \quad (15)$$

4. Let (λ_j, w_j) , $j = 1, 2, \dots, m$ be the eigenvalue-eigenvector pairs for \hat{A} . Then λ_j 's are the dynamic eigenvalues. Dynamic modes \tilde{v}_j are given by

$$\tilde{v}_j = W w_j, \quad j = 1, 2, \dots, m. \quad (16)$$

In this method, the left singular vectors W are used as the basis to compute a realization of the DMD operator, which is \hat{A} . In fact, column vectors in W form an orthogonal basis which enhances the numerical stability of the projection process (the term $W^* Y$ in step 3). As a result, SVD-enhanced DMD has become the standard choice of DMD in practice. Note that in case that X is full rank and λ_j 's are distinct, the dynamic modes and eigenvalues computed by the above two algorithms are the same [19].

The Exact DMD algorithm generalizes the SVD-enhanced algorithm to the case where different observables are measured at different times and the sampling of the data might be non-sequential.

For example, let $f_i : M \rightarrow \mathbb{R}$, $i = 1, 2, \dots, n$, denote n observables on the dynamical system (4). Then consider the data matrices

$$X = \begin{bmatrix} f_1(z_0) & f_1(z_1) & \dots & f_1(z_m) \\ f_2(z_0) & f_2(z_1) & \dots & f_2(z_m) \\ \vdots & \vdots & \ddots & \vdots \\ f_n(z_0) & f_n(z_1) & \dots & f_n(z_m) \end{bmatrix} \quad (17)$$

and

$$Y = \begin{bmatrix} f_1 \circ T(z_0) & f_1 \circ T(z_1) & \dots & f_1 \circ T(z_m) \\ f_2 \circ T(z_0) & f_2 \circ T(z_1) & \dots & f_2 \circ T(z_m) \\ \vdots & \vdots & \ddots & \vdots \\ f_n \circ T(z_0) & f_n \circ T(z_1) & \dots & f_n \circ T(z_m) \end{bmatrix}, \quad (18)$$

where $\{z_0, z_1, \dots, z_m\}$ denote a set of arbitrary states of the dynamical system in (4). The exact DMD algorithm computes the dynamic modes and eigenvalues from data matrices similar to X and Y .

Algorithm 3 (Exact DMD). Consider the data matrices X and Y defined in (17) and (18).

1. Compute the SVD of X :

$$X = W S \tilde{V}^*. \quad (19)$$

2. Form the matrix

$$\tilde{A} = W^* Y \tilde{V} S^{-1}. \quad (20)$$

3. Let (λ_j, w_j) , $j = 1, 2, \dots, m$ be the eigenvalue-eigenvector pairs for \tilde{A} . Then λ_j 's are the dynamic eigenvalues.

4. The exact dynamic modes \hat{v}_j are given by

$$\tilde{v}_j = \frac{1}{\lambda_j} Y \tilde{V} S^{-1} w_j, \quad j = 1, 2, \dots, m. \quad (21)$$

5. The projected dynamic modes \tilde{v}_j are given by

$$\tilde{v}_j = W w_j, \quad j = 1, 2, \dots, m. \quad (22)$$

The finite-dimensional operator that maps the columns of X to Y is known as the Exact DMD operator, with the explicit realization,

$$\tilde{A} = Y X^\dagger. \quad (23)$$

The matrix \tilde{A} is not actually formed in algorithm 3, however, the dynamic eigenvalues and exact dynamic modes form the eigen-decomposition of \tilde{A} . We also note that the projected dynamic modes and exact dynamic modes computed by this method coincide in the case that column space Y lie in the range of X . This condition implies the equivalence of SVD-enhanced DMD and Exact DMD when applied to X and Y matrices defined in algorithm 2.

In the next sections, we will show how DMD operators converge to a finite-dimensional representation of the Koopman operator for ergodic systems. The critical observation that enables us to do so, is the fact that vector projections in the DMD algorithm can be used to approximate the projections in the function space of observables.

3 Computation of Koopman eigenvalues and eigenfunctions in ergodic systems: the Hankel-DMD method

In this section, we propose a slight variation of companion-matrix and SVD-enhanced DMD algorithms - called the Hankel-DMD method - to compute the discrete spectrum of the Koopman operator in ergodic systems. In this method, instead of applying DMD to the snapshot matrix in (8), we apply it to a Hankel matrix made out of a sequence of observations on a scalar observable. Before we describe the mathematical setting, we review some of the recent works that motivated this approach. The relationship between the Koopman mode decomposition and the Hankel matrix representation of data, was first pointed out by [14]. It was shown that applying the Exact DMD to the Hankel data matrix recovers the same linear system, up to a similarity transformation, as the one obtained by Eigensystem Realization Algorithm (ERA). More recently, Brunton and co-workers ([20]) have proposed a new framework for Koopman analysis using the Hankel-matrix representation of data. They use the Hankel matrix to identify a linear subspace of observables which is *approximately-invariant* under the action of Koopman operator while the system trajectory is evolving on an attractor. Using this framework, they were able to extract a linear system with intermittent forcing that could be used for local predictions of chaotic systems. The following results are based on the convergence of vector projections to function projections. This observation has already been made in [21], but utilized in a different approach for computation of the Koopman spectral properties. Finally, we note that the Hankel-DMD numerical algorithm is equivalent to the Prony approximation of Koopman mode decomposition proposed in [22].

Consider the dynamics on a compact invariant set A , possibly the attractor of a dissipative dynamical system, given by the measure-preserving map $T : A \rightarrow A$. Let μ be the invariant measure with $\mu(A) = 1$, and assume that for every T -invariant set $B \subset A$, $\mu(B) = 0$ or $\mu(A - B) = 0$, i.e., the map T is ergodic on A .

Now let $f, g : A \rightarrow \mathbb{R}$ be observables that belong to the Hilbert space $\mathcal{H} := \mathcal{L}^2(A, \mu)$. The Birkhoff's ergodic theorem [23] asserts the existence of time averages of such observables over infinite time and relates it to the spatial average over the set A . More precisely,

$$\lim_{N \rightarrow \infty} \frac{1}{N} \sum_{k=0}^N f \circ T^k(z) = \int_A f d\mu, \quad \text{for almost every } z \in A. \quad (24)$$

An important consequence of this theorem is that the inner products of observables in \mathcal{H} can be approximated using the time series of observations. To see this denote by $\tilde{f}_m(z_0)$ the vector of m sequential observations made on a trajectory starting at $z_0 \in A$,

$$\tilde{f}_m(z_0) = [f(z_0), f \circ T(z_0), \dots, f \circ T^{m-1}(z_0)] \quad (25)$$

Then for almost every z_0 ,

$$\lim_{m \rightarrow \infty} \frac{1}{m} \langle \tilde{f}_m(z_0), \tilde{g}_m(z_0) \rangle = \lim_{m \rightarrow \infty} \frac{1}{m} \sum_{k=0}^m (fg^*) \circ T^k(z_0) = \int_A fg^* d\mu = \langle f, g \rangle_{\mathcal{H}} \quad (26)$$

where we have used the ergodicity in the second equality. Note that $\langle \cdot, \cdot \rangle$ is used for vector inner product while $\langle \cdot, \cdot \rangle_{\mathcal{H}}$ is the inner product on \mathcal{H} .

The finite vector of observations $\tilde{f}_m(z_0)$ provides a spatial sample of the observable f over the trajectory starting at $z_0 \in A$, and moreover, it can be used to approximate the projection of such functions onto each other according to (26). Now consider the longer sequence of observations,

given as follows

$$\tilde{f}_{m+n} = [f(z_0), f \circ T(z_0), \dots, f \circ T^{m-1}(z_0), \dots, f \circ T^{m+n-1}(z_0)]$$

which could be rearranged into the Hankel matrix form,

$$\begin{aligned} \tilde{H} &= \begin{pmatrix} f(z_0) & f \circ T(z_0) & \dots & f \circ T^n(z_0) \\ f \circ T(z_0) & f \circ T^2(z_0) & \dots & f \circ T^{n+1}(z_0) \\ \vdots & \vdots & \ddots & \vdots \\ f \circ T^{m-1}(z_0) & f \circ T^m(z_0) & \dots & f \circ T^{m+n-1}(z_0) \end{pmatrix} \\ &= (\tilde{f}_m, U\tilde{f}_m, \dots, U^n\tilde{f}_m). \end{aligned} \quad (27)$$

The Hankel matrix \tilde{H} gives an approximation of the Krylov sequence of the Koopman operator,

$$\mathcal{K}_n(U, f) := [f, Uf, \dots, U^n f].$$

by sampling the value of functions $U^j f$, $j = 0, 1, \dots, n$ along the trajectory starting at z_0 . Let us consider the case when $\mathcal{K}_n(U, f)$ spans a k -dimensional subspace of \mathcal{H} with $k < n$. This implies that $U^n f$ is linearly dependent on the sequence of functions

$$X := [f, Uf, \dots, U^{n-1}f]$$

and therefore the future iterates U^{n+j} , $j = 1, 2, \dots$ would also be linearly dependent on X . This means that k -dimensional subspace $\text{span}\{X\}$ is invariant under the action of the Koopman operator. We can reduce the study of the Koopman operator to this subspace, which makes it obvious that the Koopman operator has discrete eigenvalues. Moreover, these eigenvalues lie on the unit circles, since Koopman operator is unitary for ergodic dynamical systems [4].

Consider applying the companion-matrix DMD algorithm (algorithm 1) to the first $k+1$ columns of \tilde{H} defined in (27). The following proposition shows that the computed dynamic modes and eigenvalues converge to the Koopman eigenvalues and eigenfunctions as $m \rightarrow \infty$:

Proposition 1 (Convergence of the companion-matrix Hankel-DMD algorithm). *Let $\mathcal{K}_n(U, f)$ span a k -dimensional subspace of \mathcal{H} with $k < n$.*

Then, for almost every z_0 , as $m \rightarrow \infty$

- (a) *The dynamic eigenvalues converge to the Koopman eigenvalues associated with the k -dimensional subspace.*
- (b) *The dynamic modes converge to the Koopman eigenfunctions on the trajectory starting at z_0 .*

Proof. Consider the first k linearly independent elements of $\mathcal{K}_n(U, f)$,

$$(f, Uf, \dots, U^{k-1}f) \quad (28)$$

These k functions provide a basis for the invariant subspace, and the restriction of Koopman operator to this subspace can be (exactly) realized as the companion matrix

$$C = \begin{pmatrix} 0 & 0 & \dots & 0 & c_0 \\ 1 & 0 & \dots & 0 & c_1 \\ 0 & 1 & \dots & 0 & c_2 \\ \vdots & \vdots & \ddots & \vdots & \vdots \\ 0 & 0 & \dots & 1 & c_{k-1} \end{pmatrix}$$

where the last column represent the coordinates of the function $U^k f$ in the basis and it is given by the skew projection of the following form

$$\begin{bmatrix} c_0 \\ c_1 \\ \vdots \\ c_{k-1} \end{bmatrix} = G^{-1} \begin{bmatrix} \langle f, U^k f \rangle_{\mathcal{H}} \\ \langle Uf, U^k f \rangle_{\mathcal{H}} \\ \vdots \\ \langle U^{k-1}f, U^k f \rangle_{\mathcal{H}} \end{bmatrix} \quad (29)$$

where G is the Gramian matrix of the basis given by

$$G_{ij} = \langle U^{i-1}f, U^{j-1}f \rangle_{\mathcal{H}}.$$

Now consider the numerical companion-matrix DMD algorithm. We first let $X = (\tilde{f}_m, U\tilde{f}_m, \dots, U^{k-1}\tilde{f}_m)$. When applied to the first $k+1$ columns of \tilde{H} , the algorithm seeks the eigenvalues of the companion matrix

$$\tilde{C} = \begin{pmatrix} 0 & 0 & \dots & 0 & \tilde{c}_0 \\ 1 & 0 & \dots & 0 & \tilde{c}_1 \\ 0 & 1 & \dots & 0 & \tilde{c}_2 \\ \vdots & \vdots & \ddots & \vdots & \vdots \\ 0 & 0 & \dots & 1 & \tilde{c}_{k-1} \end{pmatrix}.$$

with the coordinates $\tilde{c}_0, \tilde{c}_1, \dots, \tilde{c}_{k-1}$ given by

$$\begin{aligned} \begin{bmatrix} \tilde{c}_0 \\ \tilde{c}_1 \\ \vdots \\ \tilde{c}_{k-1} \end{bmatrix} &= X^\dagger U^k \tilde{f}_m \\ &= \tilde{G}^{-1} \begin{bmatrix} \frac{1}{m} \langle \tilde{f}_m, U^k \tilde{f}_m \rangle \\ \frac{1}{m} \langle U\tilde{f}_m, U^k \tilde{f}_m \rangle \\ \vdots \\ \frac{1}{m} \langle U^{k-1}\tilde{f}_m, U^k \tilde{f}_m \rangle \end{bmatrix} \end{aligned} \quad (30)$$

where we have used the following relationship for the Moore-Penrose pseudo-inverse of a full-rank data matrix X ,

$$X^\dagger = (X^*X)^{-1}X^* = \left(\frac{1}{m}X^*X\right)^{-1}\left(\frac{1}{m}X^*\right) := \tilde{G}^{-1}\left(\frac{1}{m}X^*\right).$$

and defined the numerical Gramian matrix by

$$\tilde{G}_{ij} = \frac{1}{m} \langle U^{i-1}\tilde{f}_m, U^{j-1}\tilde{f}_m \rangle.$$

The averaged inner products in the rightmost vector of (30) converge to the vector of Hilbert-space inner products in (29), due to (26). The same argument suggests element-wise convergence of the numerical Gramian matrix to the G in (29), i.e.,

$$\lim_{m \rightarrow \infty} \tilde{G}_{ij} = G_{ij}.$$

Furthermore

$$\lim_{m \rightarrow \infty} \tilde{G}^{-1} = \left(\lim_{m \rightarrow \infty} \tilde{G} \right)^{-1} = G^{-1}$$

We have interchanged the limit and inverting operations in the above since G is invertible (because the basis is linearly independent) and therefore its inverse is a continuous function at G . Thus the right-hand-side of (30) converges to the right-hand-side of (29) and the DMD coordinates \tilde{c}_i converge to c_i 's as $m \rightarrow \infty$. The eigenvalues of companion matrix C are the roots of a polynomial with coefficients c_i and therefore their value continuously depends on c_i . That guarantees the convergence of the eigenvalues of \tilde{C} to the eigenvalues of C as well. This proves the statement in (a).

Let v_k be the set of normalized eigenvectors of C , that is,

$$Cv_j = \lambda_j v_j, \quad \|v_j\| = 1, \quad j = 1, \dots, k.$$

These eigenvectors give the coordinates of Koopman eigenfunctions in the basis of (28). Namely, ϕ_j , $j = 1, \dots, k$ defined by

$$\phi_i = \left(f, Uf, \dots, U^{k-1}f \right) v_i, \quad i = 1, \dots, k. \quad (31)$$

are a set of Koopman eigenfunctions in the invariant subspace. Given the convergence of \tilde{C} to C and convergence of their eigenvalues, the normalized eigenvectors of \tilde{C} , denoted by \tilde{v}_j , $j = 0, 1, \dots, k$ also converge to v_j 's. Construct the set of candidate functions

$$\tilde{\phi}_i = \left(f, Uf, \dots, U^{k-1}f \right) \tilde{v}_i, \quad i = 1, \dots, k. \quad (32)$$

We will show that $\tilde{\phi}_i$ converge to ϕ_i as $m \rightarrow \infty$. Consider an adjoint basis of (28) denoted by $\{g_j\}$, $j = 0, 1, \dots, k-1$ defined such that $\langle g_i, U^j f \rangle_{\mathcal{H}} = \delta_{ij}$ with δ being the Kronecker delta. We have

$$\lim_{m \rightarrow \infty} \langle \tilde{\phi}_i, g_j \rangle_{\mathcal{H}} = \lim_{m \rightarrow \infty} \tilde{v}_{ij} = v_{ij} = \langle \phi_i, g_j \rangle_{\mathcal{H}}$$

where we have used the convergence of eigenvectors in the second equality, and v_{ij} is the i -th element of v_j . The above statement shows the *weak* convergence of the $\tilde{\phi}_j$ to ϕ_j for $j = 1, \dots, k$. However, both set of functions belong to the same *finite*-dimensional subspace and therefore weak convergence is strong convergence. Note that the j -th dynamic mode given by

$$w_i = \left(\tilde{f}_m, U\tilde{f}_m, \dots, U^{k-1}\tilde{f}_m \right) \tilde{v}_i \quad (33)$$

is the sampling of $\tilde{\phi}_j$ along the trajectory, and therefore convergence of $\tilde{\phi}_j$ means that w_j converges to the value of Koopman eigenfunction ϕ_j on the trajectory starting at z_0 . Note that the proposition is valid for almost every initial condition for which the ergodic average in (24) exists. \square

We just showed that the companion-matrix DMD operator converges to the realization of the Koopman operator in an invariant k -dimensional subspace of \mathcal{H} . It would be favorable to extend this proposition to the SVD-enhanced DMD since it is more suitable for numerical practice. The next proposition extends the above result to SVD-enhanced DMD, and furthermore, relaxes the condition of applying to only first $k+1$ columns of \tilde{H} .

Proposition 2 (Convergence of the SVD-enhanced Hankel-DMD algorithm). *Let $\mathcal{K}_n(U, f)$ span a k -dimensional subspace of \mathcal{H} with $k < n$. Consider eigenvalues and eigenmodes of the SVD-enhanced Hankel-DMD algorithm (algorithm 2) applied to the Hankel matrix $\tilde{H}_{m \times n}$ defined in (27).*

Then, for almost every z_0 , as $m \rightarrow \infty$

- (a) The dynamic eigenvalues converge to the Koopman eigenvalues.*
- (b) The dynamic modes converge to the spatial sample of associated Koopman eigenfunctions on the trajectory starting at z_0 .*

Proof. Consider the case when $n = k + 1$ and Koopman eigenvalues are distinct. Given that the rank of \tilde{H} is equal to number of non-zero eigenvalues of \tilde{G} , the convergence of \tilde{G} implies the existence of m_0 such that for every $m > m_0$, \tilde{H} is full rank. It follows from theorem 1 in [19] that the dynamic eigenvalues and modes obtained by SVD-enhanced DMD and companion-matrix DMD are the same.

We do not give the proof for the case of arbitrary eigenvalues and $n > k + 1$ here. However, in proposition 5, we show the convergence of Exact DMD which implies the convergence of SVD-enhanced DMD as well. \square

Remark 1. *The key point in the proof is the convergence of vector projections in the DMD to the projections in H following (26). In case of periodic and quasi-periodic attractors, the error of approximating the inner products by (26) is generally bounded by $|c/m|$ for some $c \in \mathbb{R}$ [24]. For strongly mixing systems, the rate of convergence slows down to c/\sqrt{m} . However for the general class of ergodic systems convergence rates cannot be established [25].*

Remark 2. *The dimension of invariant subspace (k) is often not known prior to the computation, and for a typical observable the invariant subspace associated with Koopman discrete spectrum might even be infinite-dimensional, i.e., observable can depend on a countably infinite number of Koopman eigenfunctions. In numerical applications, however, it is reasonable to assume that the observable might live in an invariant finite-dimensional subspace down to some numerical accuracy, and if n is chosen large enough, convergence can be achieved. In fact, SVD finds an orthogonal basis for finite-dimensional approximation of the observable and the SVD-enhanced DMD operator (\hat{A} in algorithm 2) approximates the realization of the Koopman operator in that finite-dimensional subspace. We will discuss the role of SVD further in section 4.*

Remark 3. *In the above results, the vectors of observations can be replaced with any sampling vectors of the observables that satisfies the convergence of inner products as in (26). For example, instead of using \tilde{f} as defined in (25), we can use the sampling vectors of the following form:*

$$\hat{f}_m(z_0) = [f(z_0), f \circ T^l(z_0), f \circ T^{2l}(z_0), \dots, f \circ T^{(m-1)l}(z_0)] \quad (34)$$

where l is a positive finite integer.

3.1 Numerical examples: periodic and quasi-periodic cavity flow

We show the application of the the Hankel-DMD method - as stated in proposition 2 - in the case of periodic and quasi-periodic attractors in high-dimensional systems. In a previous study by authors [26], the lid-driven cavity flow was shown to exhibit periodic and quasi-periodic behavior at Reynolds numbers (Re) in the range of 10000-18000. The Koopman frequencies were computed by applying an adaptive combination of FFT and harmonic averaging to the discretized field of

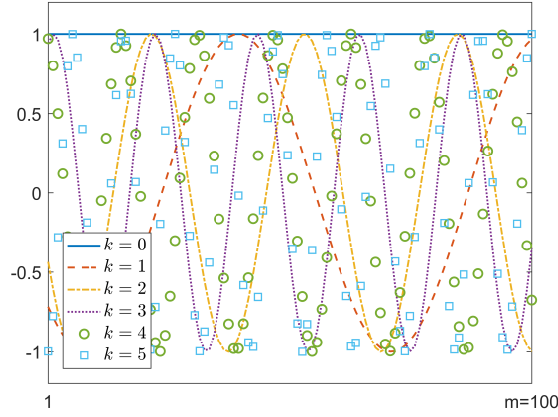


Figure 1: Real part of the computed Koopman eigenfunctions $\tilde{\phi}_k$ along the trajectory for periodic cavity flow at $Re = 13000$.

k	$\tilde{\omega}^k$	ω^k ([26])	relative error	$var(\tilde{\phi}_k - \phi_k)$
0	0	0	0	$< 1e-10$
1	1.00421	1.00423	$1.59e-5$	$1.46e-6$
2	2.00843	2.00840	$1.56e-5$	$2.25e-5$
3	3.01264	3.012629	$4.94e-6$	$< 1.00e-10$
4	4.01685	4.001680	$1.55e-5$	$< 1.00e-10$
6	6.02528	6.025257	$5.03e-6$	$< 1.00e-10$

Table 1: Comparison of the dominant Koopman frequencies and eigenfunctions for periodic cavity flow

stream function, which is an observable with 4000 values. In particular, the following cases were observed:

I. At $Re = 13000$ the flow trajectory in the state space converges to a limit cycle with basic frequency of $\omega_0 = 1.0042 \text{ rad/sec}$. The Koopman frequencies in the decomposition of observables such as velocity field and kinetic energy are multiples of the basic frequency, i.e., $k\omega_0$, $k = 0, 1, 2, \dots$

II. At $Re = 16000$, the post-transient flow is quasi-periodic with two basic frequencies $\omega_1 = 0.9762 \text{ rad/sec}$ and $\omega_2 = 0.6089 \text{ rad/sec}$. In this case, the flow trajectory wraps around a 2-torus in the state space of the flow and the Koopman frequencies are integral multiples of ω_1 and ω_2 , that is $\omega = \mathbf{k} \cdot (\omega_1, \omega_2)$, $\mathbf{k} \in \mathbb{Z}^2$.

Here we apply the Hankel-DMD method to a single-observable data - the kinetic energy - collected from post-transient simulations in each case. Let $\{E_i := E(t_0 + i\Delta t)\}$ denote the measurements on the kinetic energy of the flow at the time instants $t_0 + i\Delta t$, $i = 0, 1, 2, \dots, s$. We first build the Hankel matrix of the kinetic energy observable,

$$\tilde{H}_E = \begin{pmatrix} E_0 & E_1 & \dots & E_n \\ E_1 & E_2 & \dots & E_{n+1} \\ E_2 & E_3 & \dots & E_{n+2} \\ \vdots & \vdots & \ddots & \vdots \\ E_{m-1} & E_m & \dots & E_{m+n-1} \end{pmatrix}. \quad (35)$$

and then we apply the SVD-enhanced DMD algorithm to this matrix. In computing the SVD of the Hankel matrix (step 2 in algorithm 2), we discard the left and right singular vectors which correspond to singular values smaller than $1e-10$. Due to the discrete-time nature of the measurements, the eigenvalues computed by this method correspond to the discrete map obtained by strobing the original continuous-time dynamical system - in this case the cavity flow evolving under Navier-Stokes dynamics - at intervals of length Δt . These discrete eigenvalues $\lambda_j, j = 1, 2, \dots$ obtained by this method are related to the Koopman frequencies $\omega_j, j = 1, 2, \dots$ through the following relationship:

$$\lambda_j = e^{i\omega_j \Delta t}.$$

The dynamic modes $\tilde{\phi}_j$ obtained by this method, as suggested by the proposition, approximate the value of the associated Koopman eigenfunctions along the first m points on the trajectory of the system.

In case I, we use 200 samples of the kinetic energy signal with sampling interval of 0.1 *sec* and we set $m = n = 100$. The first Koopman frequency is zero, corresponding to the discrete eigenvalue 1, which is expected from the fact the Koopman operator always has eigenvalue 1 associated with eigenfunctions constant on the state space. In the table 1 we present frequencies obtained using the DMD-Hankel method, labeled by $\tilde{\omega}_k$, and compare with frequencies computed with the method of [26]. The basic frequency obtained by the new method is in good agreement with the results of [26]. The rest of computed Koopman frequencies are found to be integral multiples of the basic frequency with an accuracy of $\mathcal{O}(10^{-5})$. For purpose of further validation, we compare the computed eigenfunctions, with the theoretical values known from the theory for periodic and quasi-periodic attractors [27]. The Koopman eigenfunctions for limit cycling system are the Fourier basis along the limit cycle. To make this notion precise, let $s \in [0, 2\pi)$ be a parametrization of the limit cycle defined by $\dot{s} = \omega_0$. The Koopman eigenfunction associated with the Koopman frequencies $\omega_k := k\omega_0$ are given by

$$\phi_k = e^{iks}, \quad k = 1, 2, 3, \dots \quad (36)$$

The real part of the Koopman eigenfunctions $\tilde{\phi}_k$ computed via the Hankel-DMD method are shown along the trajectory in figure 1. The mean squared error in the approximation of the six eigenfunctions with largest vector energy is less than 10^{-5} , as seen from the last column in the table 1.

Table 2 shows the eigenvalues computed by applying the Hankel-DMD method to the kinetic energy data from the quasi-periodic cavity flow (case II). Note that in this example a longer sequence of observations is required to sufficiently sample the attractor which is a 2-torus. The eigenvalues shown in the table are computed using 6500 samples of the kinetic energy signal with sampling interval of 0.1 seconds, and by setting $m = 6000$ and $n = 500$. The basic frequencies can be identified manually, usually by examining the combination of the first few frequencies. Once the basic frequency vector (ω_1, ω_2) is determined, the attractor, in this case a 2-torus, can be parameterized by the time-linear coordinates $(\theta, \phi) \in [0, 2\pi)^2$, defined by

$$\begin{aligned} \theta &= \omega_1 t, \\ \phi &= \omega_2 t. \end{aligned} \quad (37)$$

The trajectory of the system on the parameterized torus is shown in figure 2. The Koopman eigenfunctions associated with the frequency $\mathbf{k} \cdot (\omega_1, \omega_2)$ are given by

$$\phi_{\mathbf{k}} = e^{i\mathbf{k} \cdot (\theta, \phi)}, \quad \mathbf{k} \in \mathbb{Z}^2. \quad (38)$$

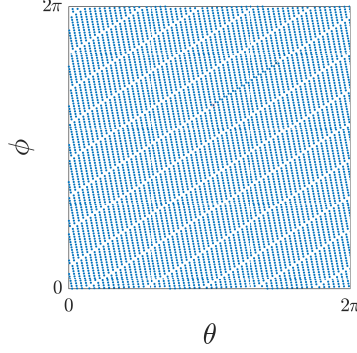


Figure 2: The trajectory of quasi-periodic flow on the time-parametrization of the torus defined in (37).

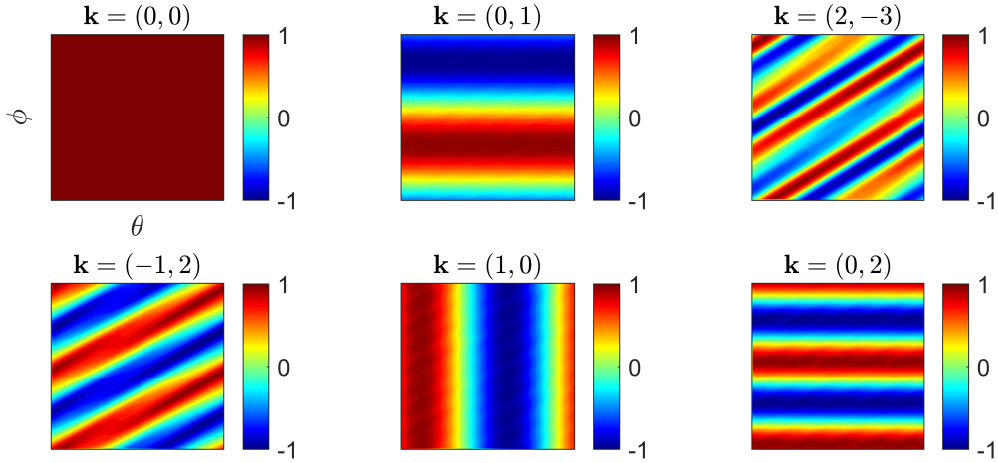


Figure 3: Real part of Koopman eigenfunctions $\tilde{\phi}_{\mathbf{k}}$ on the parameterized torus of quasi-periodic cavity flow at $Re = 16000$.

The modes obtained by Hankel-DMD method provide an approximation of the Koopman eigenfunction along the trajectory (the dots in figure 2) which could be extended to the whole torus through an interpolation process. Using this technique, we have plotted the Koopman eigenfunctions on the parameterized torus in 3. The computed value of frequencies and eigenfunctions are in good agreement with the [26] and theory (Table 2).

3.2 Extension to dissipative dynamical systems

Consider the ergodic set A , defined above, to be an attractor of the dynamical system (4) with a basin of attraction denoted by \mathcal{B} . For certain types of attractors, such as periodic, the existence of ergodic average (24) can be extended to trajectories starting almost everywhere in \mathcal{B} [28]. The only extra condition required for this is that the observable must be *continuous*. To formalize this,

k	$\tilde{\omega}^k$	ω^k ([26])	relative error	$var(\tilde{\phi}_k - \phi_k)$
(0, 0)	0	0	0	$1.64e-9$
(0, 1)	0.60891	0.60890	$1.58e-5$	$9.58e-4$
(2, -3)	0.12443	0.12598	$1.23e-2$	$1.69e-1$
(-1, 2)	0.24159	0.24149	$3.96e-4$	$1.88e-2$
(1, 0)	0.97624	0.97624	$3.68e-6$	$1.12e-3$
(0, 2)	1.21781	1.21773	$6.40e-5$	$6.29e-3$

Table 2: comparison of the dominant Koopman frequencies and eigenfunctions for quasi-periodic cavity flow

let $f : \mathcal{B} \rightarrow \mathbb{R}$ be a continuous function over \mathcal{B} . Then

$$\lim_{N \rightarrow \infty} \frac{1}{N} \sum_{k=0}^N f \circ T^k(z) = \int_A f d\mu, \quad \text{for almost every } z \in \mathcal{B}. \quad (39)$$

The convergence of inner products such as in (26) follows for continuous observables and therefore we can extend proposition 1 to the trajectories starting almost everywhere in \mathcal{B} :

Proposition 3 (Convergence of Hankel-DMD inside the basin of attraction). *Let $f : \mathcal{B} \rightarrow \mathbb{R}$ be a continuous function, and $f|_A$ belong to a k -dimensional Koopman-invariant subspace of \mathcal{H} . Consider the application of the companion-matrix and SVD-enhanced DMD (algorithms 1 and 2) to the first $k+1$ columns of Hankel matrix (27), made out of a sequence of observations on $f \circ T^i(z_0)$, $i = 0, 1, \dots, m$, with $z_0 \in \mathcal{B}$.*

Then, for almost every z_0 , as $m \rightarrow \infty$:

1. *The dynamic eigenvalues converge to the Koopman eigenvalues.*
2. *The dynamic modes converge to the value of associated eigenfunctions ϕ_j along the trajectory starting at z_0 .*

Proof. The proof of (a) is similar to proposition 1 and follows from the extension of ergodic averages to the basin of attraction. To show that the dynamic mode w_j converges to Koopman eigenfunctions along the trajectory, we need to consider the evolution of w_j under the action of the Koopman operator:

$$\begin{aligned}
\lim_{m \rightarrow \infty} U w_j &= \lim_{m \rightarrow \infty} U[\tilde{f}_m, U\tilde{f}_m, \dots, U^{k-1}\tilde{f}_m] \tilde{v}_j \\
&= \lim_{m \rightarrow \infty} [U\tilde{f}_m, U^2\tilde{f}_m, \dots, U^k\tilde{f}_m] \tilde{v}_j \\
&= \lim_{m \rightarrow \infty} [\tilde{f}_m, U\tilde{f}_m, \dots, U^{k-1}\tilde{f}_m] \tilde{C} \tilde{v}_j \\
&= \lim_{m \rightarrow \infty} [U\tilde{f}_m, U^2\tilde{f}_m, \dots, U^k\tilde{f}_m] \tilde{\lambda}_j \tilde{v}_j \\
&= \lim_{m \rightarrow \infty} \tilde{\lambda}_j w_j \\
&= \lambda_j w_j.
\end{aligned}$$

Therefore the elements of w_j are values of an eigenfunctions of the Koopman operator at eigenvalue λ_j . \square

We show an application of this extension by computing the asymptotic phase for trajectories of the Van der Pol oscillator. For definition of this problem, we closely follow the discussion in [29]. Consider the classical Van der Pol model

$$\dot{z}_1 = z_2, \quad \dot{z}_2 = \mu(1 - z_1^2)z_2 - z_1, \quad \mathbf{z} := (z_1, z_2) \in \mathbb{R}^2 \quad (40)$$

For the parameter value $\mu = 0.3$, all the trajectories in the state space \mathbb{R}^2 converge to a (stable) limit cycle Γ with the basic frequency $\omega_0 \approx 0.995$. Similar to the example of periodic flow above, we can assign to each point on the limit cycle a phase $\theta \in [0, 2\pi)$. To make this notion more precise, we let $S^t(\mathbf{z})$ denote the position of trajectory starting at \mathbf{z} at time t . We first set $\theta = 0$ for an arbitrary point $\mathbf{z}_0^\Gamma \in \Gamma$ and say $\mathbf{z}_\theta \in \Gamma$ has the phase $\theta = \omega_0 t \pmod{2\pi}$, if $S^t(\mathbf{z}_0^\Gamma) = \mathbf{z}_\theta$.

The notion of phase θ can be extended to all the points in the basin of attraction $\mathcal{B} = \mathbb{R}^2$ for the limit cycle Γ . We say the point $\mathbf{z} \in \mathcal{B}$ has phase s if

$$\lim_{t \rightarrow \infty} \|S^t(\mathbf{z}) - S^t(\mathbf{z}_\theta)\| = \lim_{t \rightarrow \infty} \|S^t(\mathbf{z}) - S^{t+\theta/\omega_0}(\mathbf{z}_0^\Gamma)\| = 0 \quad (41)$$

Roughly speaking, each $\mathbf{z} \in \mathcal{B}$ asymptotically converges to the orbit of a point on Γ and we are setting the phases of those two points equal to each other. This parametrization of the basin of attraction is valuable since it reduces (40) to a phase model which is more tractable for mathematical analysis and control strategies. It was shown in [29], that the level sets of θ in \mathcal{B} - which are called *isochrons* - coincide with the level sets of the Koopman eigenfunction associated with the Koopman frequency ω_0 . The methodology developed in [29] is to compute the Koopman eigenfunction by taking the Fourier (or harmonic) average of the continuous observable $f : \mathcal{B} \rightarrow \mathbb{R}$,

$$\phi_0(\mathbf{z}) = \lim_{T \rightarrow \infty} \frac{1}{T} \int_0^T f(S^t(\mathbf{z})) e^{-i\omega_0 t} dt, \quad (42)$$

and assigning the phase $\theta(\mathbf{z}) = \angle \phi_0(\mathbf{z})$. Note that in this method, the basic frequency must be known beforehand.

The Hankel-DMD method can be used to compute the basic frequency of the limit cycle and the corresponding eigenfunction ϕ_0 in the same computation. Consider a trajectory of (40) starting at $\mathbf{z} = (3, 3)$. Figure 4 shows the application of DMD-Hankel method to the time series of the continuous observable $f(\mathbf{z}) = z_1 + z_2$, sampled at every 0.1 second over a time interval of 35 seconds ($m = 250$ and $n = 100$). The left panel shows the agreement between that the Koopman eigenfunction ϕ_0 computed by this method, with the results of Fourier averaging (42). The right panel shows the phase $\theta = \angle \phi_0$ plotted as the color field along the trajectory.

4 Singular Value Decomposition (SVD) and Proper Orthogonal Decomposition (POD) for ergodic systems

SVD is in the core of many algorithms for analysis of data from dynamical systems including linear subspace identification method (see e.g. [30]) and some variants of DMD, such as SVD-enhanced DMD by [6] and Exact DMD by [14]. Proper Orthogonal Decomposition (POD), on the other hand, is a data analysis technique which is frequently used in study of data from complex and high-dimensional dynamical systems, and it is known that when the observables on a discrete-time dynamical system are finite-dimensional, then POD reduces to SVD [31]. Here, we establish a precise connection between these two concepts in the case of ergodic systems. Our motivation for derivation of these results is the role of SVD in the implementation of DMD algorithms, however, the orthonormal basis that is generated by this process can be used for further analysis of dynamics

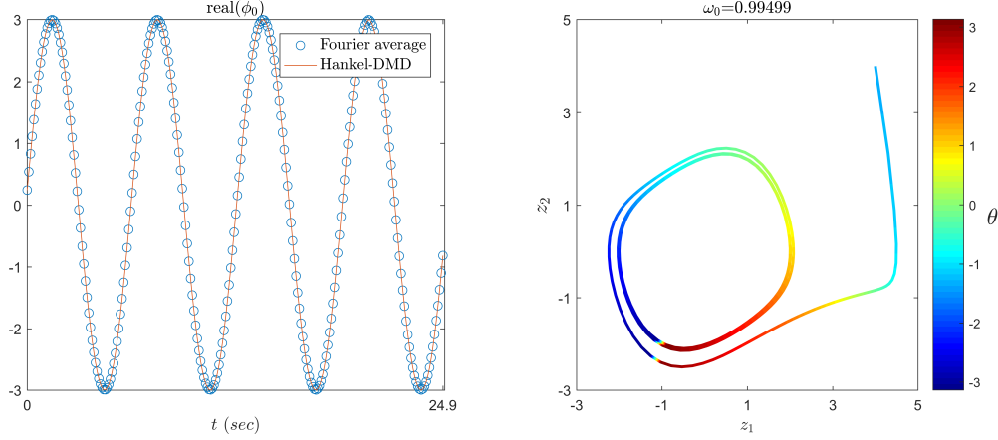


Figure 4: The Koopman eigenfunction associated with ω_0 (left), and asymptotic phase for a trajectory of Van der Pol oscillator (right). The initial conditions with the same color converge to the same orbit on the limit cycle.

in the space of observables, for example, to construct a basis for computing the eigenfunctions of the Koopman generator as in [21].

Let $F = [f_1, f_2, \dots, f_n]$ be an ensemble of observables that belong to the Hilbert space \mathcal{H} , and assume the functions in F span a k -dimensional subspace of \mathcal{H} . The Proper Orthogonal Decomposition seeks an expansion of the form

$$F = \Psi \Sigma V^*, \quad (43)$$

$$= [\psi_1, \psi_2, \dots, \psi_k] \begin{bmatrix} \sigma_1 & 0 & \dots & 0 \\ 0 & \sigma_2 & \dots & 0 \\ \vdots & \vdots & \ddots & \vdots \\ 0 & 0 & \dots & \sigma_k \end{bmatrix} \begin{bmatrix} - & v_1^* & - \\ - & v_2^* & - \\ & \vdots & \\ - & v_k^* & - \end{bmatrix}$$

where ψ_j , $j = 1, 2, \dots, k$ form an orthonormal basis for $\text{span}\{F\}$, and often called the *proper orthogonal functions* or principle components of F . The positive diagonal elements of Σ , denoted by σ_j , $j = 1, 2, \dots, k$ signify the L^2 -norm contribution of the basis element ψ_j to the F , and columns of V^* , called the *principle coordinates*, are the normalized coordinates of the functions in F with respect to the orthonormal basis. This decomposition can be alternatively written in the algebraic form

$$f_i = \sum_{j=1}^k \sigma_j \psi_j v_{ij} \quad (44)$$

If the matrix columns in (43) is rearranged such that $\sigma_1 > \sigma_2 > \dots > \sigma_k > 0$, then this decomposition minimizes the expression

$$e_p = \frac{1}{n} \sum_{i=1}^n \left\| \sum_{j=1}^p \sigma_j \psi_j V_{ji}^* - f_i \right\|_{\mathcal{H}}$$

for any $p \leq k$, over the choice of all orthonormal bases for $\text{span}\{F\}$. In the above definition, e_p denotes the average error in approximating f_i 's by truncating the sum in (44) at length p . This

property, by design, guarantees that low-dimensional representations of F using POD involves the least error compared to representation in other orthogonal bases.

An established method for computation of POD is *the method of snapshots* [32]. In this method, we first form the Gramian matrix G , defined by $G_{ij} = \langle f_i, f_j \rangle_{\mathcal{H}}$. The columns of V are the normalized eigenvectors of G associated with its non-zero eigenvalues. These non-zero eigenvalues happen to be σ_i^2 , $i = 1, 2, \dots, k$, i.e.,

$$GV = V\Sigma^2. \quad (45)$$

Since G is a symmetric real matrix, V is an orthonormal matrix and the decomposition in (43) can be easily inverted to yield the orthonormal basis functions in Ψ :

$$\Psi = FV\Sigma^{-1}.$$

The Singular Value Decomposition (SVD) has a similar structure to POD. Consider a full-rank data matrix $X_{m \times n}$ with $m > n$. Then the economy-sized singular decomposition of X is given by

$$X = WS\tilde{V}^* \quad (46)$$

$$= \begin{bmatrix} | & | & \dots & | \\ w_1 & w_2 & \dots & w_n \\ | & | & \dots & | \end{bmatrix} \begin{bmatrix} s_1 & 0 & \dots & 0 \\ 0 & s_2 & \dots & 0 \\ \vdots & \vdots & \ddots & \vdots \\ 0 & 0 & \dots & s_n \end{bmatrix} \begin{bmatrix} - & \tilde{v}_1^* & - \\ - & \tilde{v}_2^* & - \\ \vdots & \vdots & \\ - & \tilde{v}_n^* & - \end{bmatrix}$$

where W and V are orthonormal matrices and S is a diagonal matrix with positive values s_i , $i = 1, 2, \dots, n$ on its diagonals which are called singular values and ordered such that $s_1 > s_2 > \dots > s_n$. The columns of W and V are also called left and right singular vectors of X respectively (see [18] for more properties of SVD). One common practice in data analysis is obtain a low-dimensional representation of X by keeping a low number of largest singular values, e.g., s_i , $i = 1, 2, 3, \dots, k$ and discard the rest of singular values and their associated singular vectors from the above expansion. This k -dimensional approximation of X , is in fact a projection of columns of X onto range of the first k columns of W .

In this work, we would be interested in the case where $m \rightarrow \infty$ and for reasons that will become clear in the next proposition, we give a new definition of such k -dimensional approximation which differs from above, only for computation of the first k left singular vectors.

Definition 1 (k -dimensional SVD approximation). *We call*

$$X \approx \hat{W}\hat{S}\hat{V}^* \quad (47)$$

a k -dimensional SVD approximation of the matrix $X_{m \times n}$ when it is computed as follows:

- (a) *The singular values s_i , $i = 1, 2, \dots, k$ are the square root of the k largest eigenvalues of X^*X .*
- (b) *The right singular vectors in $\hat{V}_{n \times k}$ are normalized eigenvectors of X^*X associated with the k largest eigenvalue.*
- (c) *The left singular vectors are given by $\hat{W} = X\hat{V}\hat{S}^{-1}$.*

Note that the singular values and right singular vectors in this definition is the same as standard SVD in (46). In case that $k = n$, the left singular vectors are also the same. The next proposition shows the connection between POD and this slightly-redefined version of SVD.

Proposition 4 (Convergence of SVD to POD for ergodic systems). *Let $F = [f_1, f_2, \dots, f_n]$ be an ensemble of observables on the discrete dynamical system in (4) with T being ergodic. Assume F spans a k -dimensional subspace of \mathcal{H} and let*

$$F = \Psi \Sigma V^*,$$

be the POD of F . Now consider the data matrix,

$$\tilde{F} = \begin{pmatrix} f_1(z_0) & f_2(z_0) & \dots & f_n(z_0) \\ f_1 \circ T(z_0) & f_2 \circ T(z_0) & \dots & f_n T(z_0) \\ \vdots & \vdots & \ddots & \vdots \\ f_1 \circ T^{m-1}(z_0) & f_2 \circ T^{m-1}(z_0) & \dots & f_n T(z_0) \end{pmatrix} \quad (48)$$

and let

$$\frac{1}{\sqrt{m}} \tilde{F} \approx \hat{W} \hat{S} \hat{V}^*$$

be the k -dimensional SVD approximation of $(1/\sqrt{m})\tilde{F}$ as in definition 1.

Then as $m \rightarrow \infty$,

(a) $\hat{S} \rightarrow \Sigma$.

(b) $\hat{V} \rightarrow V$.

(c) *The j -th column of the matrix $\sqrt{m}\hat{W}$ (left singular vectors) converge to the value of POD basis function ψ_j , along the trajectory starting at almost every z_0 .*

Proof. (a) The diagonal elements of \hat{S} , by definition, are the square root of the k largest eigenvalues of the numerical Gramian matrix

$$\tilde{G} := \left(\frac{1}{\sqrt{m}}\tilde{F}\right)^* \left(\frac{1}{\sqrt{m}}\tilde{F}\right) = \frac{1}{m} \tilde{F}^* \tilde{F}.$$

As shown in the proof of proposition 1, the assumption of ergodicity on T implies the convergence of \tilde{G} to the Gramian matrix G in (45) as $m \rightarrow \infty$. Therefore the eigenvalues of \tilde{G} converge to those of G . Now denote by λ_j , $j = 1, 2, \dots, k$ the k eigenvalues of \tilde{G} that converge to positive eigenvalues of G , and denote by λ_j , $j = k+1, k+2, \dots, n$ the eigenvalues of \tilde{G} that converge to zero. The convergence of eigenvalues means that there exists m_0 such that for any $m > m_0$, the singular values $s_j = \sqrt{\lambda_j}$, $j = 1, 2, \dots, k$ are larger than $s_j = \sqrt{\lambda_j}$, $j = k+1, k+2, \dots, n$ and therefore s_j , $j = 1, 2, \dots, k$ occupy the diagonal of \hat{S} , which completes the proof of statement in (a).

Now consider the normalized eigenvectors of \tilde{G} associated with λ_j , $j = 1, 2, \dots, k$. For $m > m_0$, these eigenvectors form the columns of \hat{V} , and since they converge to normalized eigenvectors of G , the statement in (b) is true as well.

To show that (c) is true, we first construct the candidate functions $\tilde{\psi}_j$, $j = 1, 2, \dots, k$, given by

$$\tilde{\Psi} := [\tilde{\psi}_1, \tilde{\psi}_2, \dots, \tilde{\psi}_k] = F \hat{V} \hat{S}^{-1}, \quad (49)$$

Then we compute the inner product matrix P defined by $P_{i,j} = \langle \psi_i, \tilde{\psi}_j \rangle$ and consider its limit,

$$\begin{aligned} \lim_{m \rightarrow \infty} P &= \lim_{m \rightarrow \infty} \Psi^* \tilde{\Psi} = \lim_{m \rightarrow \infty} (FV\Sigma^{-1})^* F \hat{V} \hat{S}^{-1} = \lim_{m \rightarrow \infty} \Sigma^{-1} V^* F^* F \hat{V} \hat{S}^{-1} \\ &= \Sigma^{-1} V^* F^* F \lim_{m \rightarrow \infty} \hat{V} \hat{S}^{-1} = \Sigma^{-1} V^* G \left(\lim_{m \rightarrow \infty} \hat{V} \hat{S}^{-1} \right) \\ &= \Sigma^{-1} V^* G V \Sigma^{-1} = \Sigma^{-1} V^* V \Sigma^2 \Sigma^{-1} = I. \end{aligned}$$

In the second to last equality we have used (45). This calculation shows that $\tilde{\psi}_j$'s are weakly convergent to ψ_j 's, and since they belong to the same finite-dimensional space, that implies strong convergence as well. Next, note that columns of \tilde{F} can be written as spatial samples of columns of F along the trajectory starting at z_0 , i.e.,

$$\tilde{F}_j = [f_j(z_0), f_j \circ T(z_0), \dots, f_j \circ T^{m-1}(z_0)]^T. \quad (50)$$

where \tilde{F}_j denotes the j -th column of \tilde{F} . The matrix of left singular vectors \hat{W} is given by

$$\hat{W} = \frac{1}{\sqrt{m}} \tilde{F} \hat{V} \hat{S}^{-1}, \quad (51)$$

and if we let \hat{W}_j be its j -th vector, then

$$\begin{aligned} \lim_{m \rightarrow \infty} \sqrt{m} \hat{W}_j &= \lim_{m \rightarrow \infty} \tilde{F} \tilde{V}_j \tilde{S}_j^{-1} = \lim_{m \rightarrow \infty} [\tilde{F}_1, \tilde{F}_2, \dots, \tilde{F}_n] \tilde{V}_j \tilde{S}_j^{-1} \\ &= \lim_{m \rightarrow \infty} [\tilde{\psi}_j(z_0), \tilde{\psi}_j(T(z_0)), \dots, \tilde{\psi}_j(T^{m-1}(z_0))]^T \\ &= [\psi_j(z_0), \psi_j(T(z_0)), \dots]^T. \end{aligned}$$

Note that in the third equality we have used the definition in (49). \square

Now we consider the special case where F is replaced with the Hankel matrix of measurements on a single observable.

Corollary 1. *Let \tilde{H} denote the Hankel matrix of measurements on observable f as defined in (27). Let $(\frac{1}{\sqrt{m}})\tilde{H} = W\tilde{S}\tilde{V}^*$ be the k -dimensional SVD of \tilde{H} , defined in prop. 4. Now consider the POD of the Krylov sequence $\mathcal{K} := [f, Uf, \dots, U^{n-1}f]$ which spans a k -dimensional subspace of \mathcal{H} , given by $\mathcal{K} = \Psi\Sigma V^*$.*

Then as $m \rightarrow \infty$,

- (a) *the matrix of right singular vectors \tilde{V} converges to the matrix of principle coordinates V ,*
- (b) *the j -th column of the matrix $\sqrt{m}W$ converge to the value of proper orthogonal function Ψ_j , along the trajectory starting at almost every z_0 .*

Alternatively, if we increase the number of columns in \tilde{H} , such that $n \rightarrow \infty$

- (c) *the matrix of right singular vectors \tilde{W} converges to the matrix of principle coordinates V ,*
- (d) *the j -th column of the matrix $\sqrt{m}V$ converges to the value of proper orthogonal function Ψ_j , along the trajectory starting at almost every z_0 .*

Proof. The assertions in (a) and (b) are just restatement of prop. 4 when \tilde{F} is replaced by \tilde{H} . The statements in (c) and (d) follow from the symmetric structure of the Hankel matrix, i.e., \tilde{H} with $n \rightarrow \infty$ is the transpose of \tilde{H} with $m \rightarrow \infty$, and therefore their singular values are the same whereas the right singular vectors and left singular vectors are swapped. \square

Using the above results, we are able to construct an orthonormal basis on the ergodic dynamical systems and track the evolution of observables in \mathcal{H} . Using corollary 1, for example, one can reduce the study of the Krylov sequence $[f, Uf, \dots, U^{n-1}f]$ to considering the evolution of their finite-dimensional principle coordinates stacked in V^* . Since U is a linear operator, we can represent its action by a linear mapping between the columns of V^* and compute its eigenfunctions and eigenvalues restricted to invariant finite-dimensional subspaces. We will use this approach in the next section, when we introduce a new variant of the Exact DMD algorithm for computation of Koopman spectrum from multiple observables.

4.1 Numerical example: construction of POD basis on chaotic Lorenz attractor

We use the results in corollary 1 to construct an orthonormal basis on the well known chaotic attractor of the Lorenz system [33]. The chaotic Lorenz attractor is proven to have the mixing property which implies ergodicity [34]. Our motivation for this example, however, comes from the recent work in [20] which combines the Koopman operator theory and Hankel matrix representation of the data to construct linear systems for prediction of chaotic systems such as Lorenz model. The Lorenz system given by

$$\begin{aligned}\dot{z}_1 &= \sigma(z_2 - z_1), \\ \dot{z}_2 &= z_1(\rho - z_3) - z_2, \\ \dot{z}_3 &= z_1 z_2 - \beta z_3,\end{aligned}$$

with $[z_1, z_2, z_3] \in \mathbb{R}^3$ is known to possess a stable chaotic attractor for parameter values $\sigma = 10$, $\rho = 28$ and $\beta = 8/3$. First, we sample the value of observable $f(\mathbf{z}) = z_1$ every 0.01 seconds on a random trajectory, and then form a tall Hankel matrix as in (27) with $m = 10000$ and $n = 100$. Figure 5 shows the values of first six columns of W which approximate the POD orthonormal basis on the attractor. The corresponding principle coordinates, shown in fig. 6, approximate the principle coordinates of $\mathcal{K} = [f, Uf, \dots, U^{n-1}f]$ in the POD basis. We make note that the basis functions $\tilde{\psi}_j$, $j = 1, 2, \dots, 6$ and their associated singular values show little change with m for $m \geq 10000$.

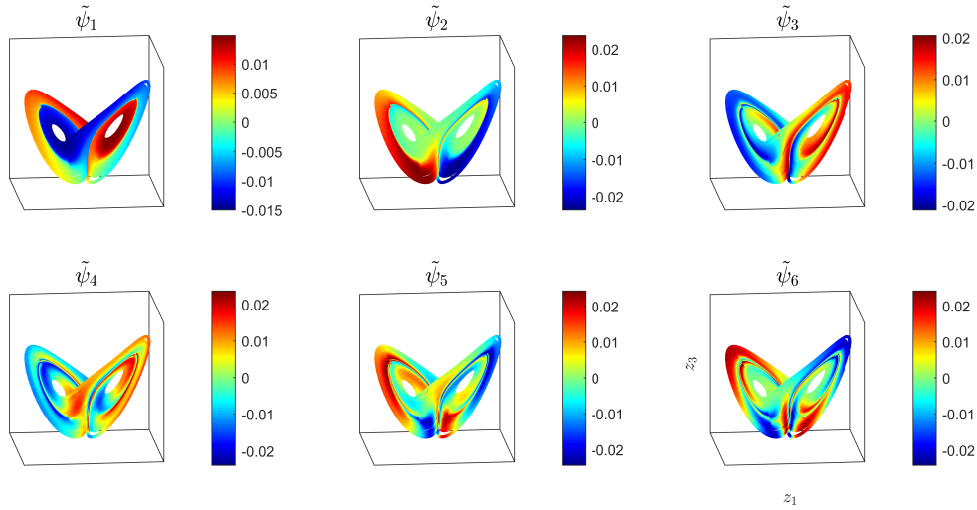


Figure 5: The POD basis on the Lorenz attractor computed using corollary 1. The observable is $f(z_1, z_2, z_3) = z_1$ and the Hankel matrix has the dimensions $m = 5000$ and $n = 100$.

In mixing attractors such as Lorenz, the only discrete eigenvalue for the Koopman operator is $\lambda = 1$ which is associated with eigenfunctions that are constant almost everywhere on the attractor. In this case, the Koopman operator cannot have any invariant finite-dimensional subspace other than span of almost-everywhere constant functions. As a result, for a typical observable f , the Krylov sequence $\mathcal{K} = [f, Uf, \dots, U^{n-1}f]$ is always n -dimensional and growing with iterations of U . This observation shows that despite the fact that evolution of principle coordinates is linear, there is no finite-dimensional linear system that can describe their evolution.

Brunton et al. [20] have used a similar framework to construct a low-dimensional linear system with intermittent forcing that emulates the dynamics of observables in several examples of chaotic

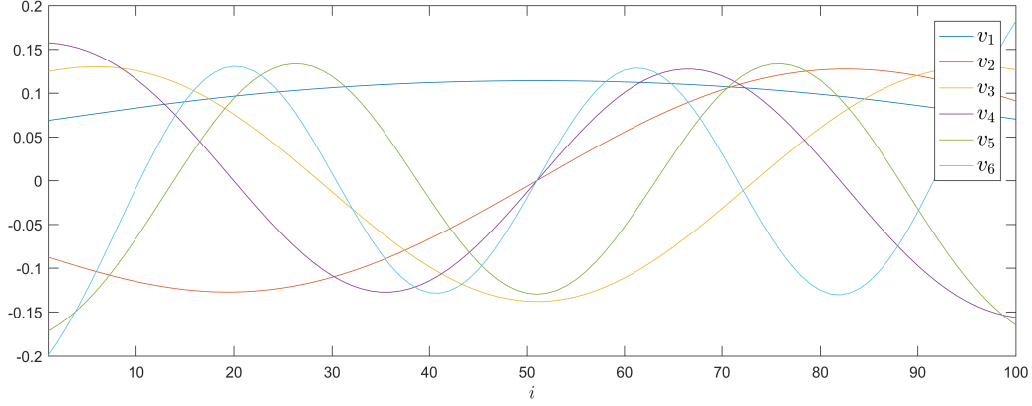


Figure 6: The principle coordinates for $[f, Uf, \dots, U^i f, \dots, U^{100} f]$ with $f(z_1, z_2, z_3) = z_1$ in the POD basis shown in figure 5.

systems. They form a Hankel matrix out of measurements on an observable and then by applying a judiciously-chosen order of truncation for SVD, they extract the so-called eigen-time-delay embedding coordinates for the observable. These eigen-delay-embedding coordinates are the right singular vectors for an extremely-fat Hankel matrix (i.e., $n \gg m$), and as a result of corollary 1(d), they can be interpreted as an approximation to the pointwise evolution of proper orthogonal functions,

$$V_B^* \approx \begin{bmatrix} \psi_1(z_0) & \psi_1 \circ T(z_0) & \dots & \psi_1 \circ T^{n-1}(z_0) \\ \psi_2(z_0) & \psi_2 \circ T(z_0) & \dots & \psi_2 \circ T^{n-1}(z_0) \\ \vdots & \vdots & \ddots & \vdots \\ \psi_r(z_0) & \psi_r \circ T(z_0) & \dots & \psi_r \circ T^{n-1}(z_0) \end{bmatrix}$$

By applying a sparse system identification method (SINDy [35]), it was found that the evolution of eigen-time-delay coordinates in chaotic systems, such as Lorenz attractor, can be described by a low-dimensional linear system being forced by an intermittent signal. This interpretation is consistent with the general framework of Koopman operator theory, since the columns of V_B^* are undergoing the action of the Koopman operator, which is linear, but since there is no finite-dimensional invariant subspace of the Koopman operator for mixing attractors, no closed linear system can describe the evolution of observables in V^* .

5 Exact DMD and extension of Hankel-DMD to multiple observables

In this section, we develop a method that uses Exact DMD (algorithm 3) to extract Koopman spectrum from measurements on multiple observables. We first describe the functional setting for this method and then state a proposition that proves the convergence. Let $F_1 =: [f_1, f_2, \dots, f_n]$ denote a set of observables defined on the discrete dynamical system (4). We make the assumption that F_1 spans a k -dimensional subspace of \mathcal{H} , with $k \leq n$, which is invariant under the Koopman operator. Also denote by $F_2 =: [Uf_1, Uf_2, \dots, Uf_n]$ the image set of those observables under the action of the Koopman operator. We seek to realize the Koopman operator, restricted to this subspace, as a k -by- k matrix, given the knowledge of F_1 and F_2 .

Let

$$F_1 = \Psi \Sigma V^*. \quad (52)$$

be the POD of ensemble F_1 with $\Psi = [\psi_1, \psi_2, \dots, \psi_k]$ denoting the POD orthonormal basis. Since F_1 spans an invariant subspace, the functions in F_2 must also belong to the same subspace and their coordinates in the POD basis can be obtained by orthonormal projection, i.e.,

$$\Omega = \Psi^* F_2. \quad (53)$$

The restriction of the Koopman operator to the invariant subspace $\text{span}\{\Psi\}$ is then given by a square matrix, A , that maps the columns of ΣV^* to Ω . The following lemma, which summarizes some of the results in [14], gives the explicit form of matrix A and asserts its uniqueness under the prescribed condition on F_1 and F_2 .

Lemma 1. *Let $X_{k \times n}$ with $n \geq k$ be a matrix whose range is equal to \mathbb{R}^k . Let $Y_{k \times n}$ be another matrix which is linearly consistent with X , i.e., whenever $Xc = 0$, then $Yc = 0$ as well. Then the Exact DMD operator $A := YX^\dagger$ is the unique matrix that satisfies $AX = Y$.*

Proof. First, we note that condition of X and Y being linearly consistent implies that A as defined above satisfies $AX = Y$ (theorem 2 in [14]). To see the uniqueness, let \tilde{A} be another matrix which satisfies $\tilde{A}X = Y$. Now let $b \in \mathbb{R}^k$ be an arbitrary vector. Given that X spans \mathbb{R}^k , we can write $b = Xd$. Consequently,

$$\tilde{A}b = \tilde{A}Xd = Yd = AXd = Ab,$$

which means that action of A and \tilde{A} on all elements of \mathbb{R}^k is the same, therefore $\tilde{A} = A$. \square

To see that ΣV^* and Ω satisfy the conditions of the lemma, we first note that F_1 spans the k -dimensional invariant subspace, and the decomposition in (52) implies that ΣV^* must span \mathbb{R}^k . Next, note that F_1 and F_2 are linearly consistent, i.e, whenever $F_1 \cdot c = 0$, then $F_2 \cdot c = U F_1 \cdot c = U(F_1 \cdot c) = U(0) = 0$. This implies that the coordinates of F_1 and F_2 in the mutual orthogonal basis Ψ is also going to be linearly consistent:

$$\Sigma V^* c = 0 \Rightarrow \Psi \Sigma V^* c = F_1 \cdot c = 0 \Rightarrow F_2 \cdot c = \Psi \Omega c = 0 \Rightarrow \Omega c = 0, \quad (54)$$

hence the linear consistency of Ω with ΣV^* . Therefore, the Koopman operator restricted to the invariant subspace is represented by the matrix

$$A = \Omega(\Sigma V^*)^\dagger = \Omega V \Sigma^{-1}, \quad (55)$$

where we have used the facts that Σ is diagonal, and V is orthonormal. Let (w_j, λ_j) , $j = 1, 2, \dots, k$ denote the eigenvectors-eigenvalues pairs of A . Then λ_j 's are the Koopman eigenvalues and the associated Koopman eigenfunctions are given by

$$\phi_j = \Psi w_j, \quad j = 1, 2, \dots, k. \quad (56)$$

Now we can assert the convergence of Exact DMD method to compute Koopman eigenvalues and eigenfunctions given the measurements of functions in F_1 and F_2 on ergodic systems.

Proposition 5 (Convergence of Exact DMD for ergodic systems). *Let $F_1 = [f_1, f_2, \dots, f_n]$ denote a set of observables that span a k -dimensional invariant subspace of the Koopman operator with $k < n$. Now consider applying the Exact DMD (algorithm 3) to the data matrices*

$$X = \begin{bmatrix} f_1(z_0) & f_2(z_0) & \dots & f_n(z_0) \\ f_1 \circ T(z_0) & f_2 \circ T(z_0) & \dots & f_n \circ T(z_0) \\ \vdots & \vdots & \ddots & \vdots \\ f_1 \circ T^{m-1}(z_0) & f_2 \circ T^{m-1}(z_0) & \dots & f_n \circ T^{m-1}(z_0) \end{bmatrix}$$

and

$$Y = \begin{bmatrix} f_1 \circ T(z_0) & f_2 \circ T(z_0) & \dots & f_n \circ T(z_0) \\ f_1 \circ T^2(z_0) & f_2 \circ T^2(z_0) & \dots & f_n \circ T^2(z_0) \\ \vdots & \vdots & \ddots & \vdots \\ f_1 \circ T^m(z_0) & f_2 \circ T^m(z_0) & \dots & f_n \circ T^m(z_0) \end{bmatrix}$$

with a k -dimensional SVD approximation (definition 1) used in step 2.

Then, for almost every z_0 , as $m \rightarrow \infty$:

1. The dynamic eigenvalues converge to the Koopman eigenvalues.
2. The j -th column of the matrix of projected dynamic modes $\sqrt{m}L$ converges to value of the Koopman eigenfunction ϕ_j along the trajectory starting at z_0 .

Proof. We first show that the matrix \tilde{A} constructed in the step 3 of the algorithm converges to the matrix A described above as $m \rightarrow \infty$. Let $X = WS\tilde{V}$, then it follows from the proof of proposition 4 that $S/\sqrt{m} \rightarrow \Sigma$ and $\tilde{V} \rightarrow V$ as $m \rightarrow \infty$. Then

$$\lim_{m \rightarrow \infty} \tilde{A} = \lim_{m \rightarrow \infty} W^*Y\tilde{V}S^{-1} = \left(\lim_{m \rightarrow \infty} \frac{1}{\sqrt{m}} W^*Y \right) V\Sigma^{-1}. \quad (57)$$

We will show that $\tilde{\Omega} := 1/\sqrt{m}W^*Y$ converges to Ω as $m \rightarrow \infty$. To this end, recall the candidate functions in $\tilde{\Psi}$ defined in proof of proposition 4. We see that

$$\tilde{\Omega}_{i,j} = \frac{1}{\sqrt{m}} W_i^* Y_j = \frac{1}{m} \sum_{l=0}^{m-1} (\tilde{\psi}_i \circ T^l(z_0))^* (U f_j \circ T^l(z_0)) := \frac{1}{m} \sum_{l=0}^{m-1} \tilde{\psi}_i^{l*} U f_j^l \quad (58)$$

Since $\tilde{\psi}_i$'s are defined by linear combination of functions in F , they lie in the span of basis in Ψ . In fact, we have

$$\tilde{\psi}_i = \sum_{q=1}^k P_{i,q} \psi_q, \quad (59)$$

where $P_{i,q}$ denotes an element of the orthogonal projection matrix P defined in the proof of proposition 4. The computation in (50) shows that as $m \rightarrow \infty$, we have $P_{i,q} \rightarrow 0$ if $q \neq i$ and $P_{i,i} \rightarrow 1$.

Now we replace $\tilde{\psi}_i$ in (58) with its expansion in (59), while considering the term

$$\begin{aligned}
d_1 &:= \tilde{\Omega}_{i,j} - \frac{1}{m} \sum_{l=0}^{m-1} (\psi_i \circ T^l(z_0))^* (U f_j \circ T^l(z_0)), \\
&= \tilde{\Omega}_{i,j} - \frac{1}{m} \sum_{l=0}^{m-1} \psi_i^{l*} U f_j^l, \\
&= \sum_{q=1}^k P_{i,q} \frac{1}{m} \sum_{l=0}^{m-1} \psi_q^{l*} U f_j^l - \frac{1}{m} \sum_{l=0}^{m-1} \psi_i^{l*} U f_j^l, \\
&= \sum_{q=1, q \neq i}^k P_{i,q} \frac{1}{m} \sum_{l=0}^{m-1} \psi_q^{l*} U f_j^l + (P_{i,i} - 1) \frac{1}{m} \sum_{l=0}^{m-1} \psi_i^{l*} U f_j^l.
\end{aligned} \tag{60}$$

The convergence of sums over l in the last line is given by (26). Combining that with the convergence of $P_{i,q}$'s, we can conclude that for every $\epsilon > 0$, there exists m_1 such that for any $m > m_1$, we have $|d_1| < \epsilon/2$. Now consider the term

$$\begin{aligned}
d_2 &= \frac{1}{m} \sum_{l=0}^{m-1} \psi_i^{l*} U f_j^l - \Omega_{i,j} \\
&= \frac{1}{m} \sum_{l=0}^{m-1} \psi_i^{l*} U f_j^l - \langle \psi_i, U f_j \rangle.
\end{aligned} \tag{61}$$

The convergence in (26) again implies that for every $\epsilon > 0$ there exists an m_2 such that for any $m > m_2$, we have $|d_2| < \epsilon$. Now it becomes clear that

$$|\tilde{\Omega}_{i,j} - \Omega_{i,j}| = |d_1 + d_2| \leq |d_1| + |d_2| = \epsilon, \tag{62}$$

for any $m > \max(m_1, m_2)$. This proves the convergence of $\tilde{\Omega}$ to Ω , which, by revisiting (57), means

$$\lim_{m \rightarrow \infty} \tilde{A} = A. \tag{63}$$

The eigenvalues of \tilde{A} converge to the eigenvalues of A which are the Koopman eigenvalues. Let \tilde{w}_j , $j = 1, 2, \dots, k$ denote the normalized eigenvectors of \tilde{A} , and define the candidate functions $\tilde{\phi}_j = \tilde{\Psi} \tilde{w}_j = \Psi P \tilde{w}_j$. Given that P converges to I and \tilde{w}_j converges to w_j as $m \rightarrow \infty$, it follows that $\tilde{\phi}_j$ strongly converge to the Koopman eigenfunctions $\phi_j = \Psi w_j$.

Now note that $\sqrt{m} L_j = \sqrt{m} U \tilde{w}_j$ is the sampling of candidate eigenfunction $\tilde{\phi}_j$ along the trajectory and therefore it converges to the sampling of the Koopman eigenfunction ϕ_j as $m \rightarrow \infty$. \square

Remark 4. Usually it is not known whether the observables in F span an invariant subspace. In that case, it would be beneficial to supplement the observables with their image under the action of the Koopman operator. For example, let f and g be the only observables that could be measured on a dynamical system. Then we can let $F_1 = [f, Uf, \dots, U^{l-1}f, g, Ug, \dots, U^{q-1}g]$. In such case, the data matrices would contain blocks of Hankel matrices,

$$X = [\tilde{H}_f \quad \tilde{H}_g], \quad Y = [U \tilde{H}_f \quad U \tilde{H}_g], \tag{64}$$

where $U\tilde{H}$ denotes the Hankel matrix which is shifted one step forward in time. The above proposition guarantees the convergence of the Exact DMD method if p and q are chosen large enough, e.g., $l, q > k + 1$ where k is the dimension of the invariant subspace containing f and g .

In numerical practice, however, the block Hankel matrices need some scaling. For instance assume $\|g\|_{\mathcal{H}} \ll \|f\|_{\mathcal{H}}$. The POD basis that corresponds to the measurements on g is associated with smaller singular values and might be discarded through a low-dimensional SVD approximation of X . To remedy this issue, we can use the fact that the ratio of the norm between observables in ergodic systems can be approximated from the measurements:

$$\alpha := \frac{\|f\|_{\mathcal{H}}}{\|g\|_{\mathcal{H}}} = \lim_{m \rightarrow \infty} \frac{\|\tilde{f}_m\|}{\|\tilde{g}_m\|}, \quad (65)$$

where \tilde{f}_m and \tilde{g}_m are the observation vectors defined in (25). The scaled data matrices in that case become

$$X = [\tilde{H}_f \quad \alpha \tilde{H}_g], \quad Y = [U\tilde{H}_f \quad \alpha U\tilde{H}_g]. \quad (66)$$

We call this technique the Exact Hankel-DMD method.

5.1 Numerical example: quasi-periodic cavity flow

We show the application of the Exact Hankel-DMD by revisiting the example of quasi-periodic flow in section 3.1. Let $\{G_i := G(t_0 + i\Delta t)\}$ to be the set of measurements of the value of the stream function at a point on the flow domain ($x = y = 0.3827$ in the domain defined in [26]). Also let E be the kinetic energy of the flow. We use the Hankel matrices of observations on G and E , by setting $m = 6000$ and $n = 500$ and form the data matrices

$$X = [\tilde{H}_E \quad \tilde{\alpha} \tilde{H}_G], \quad Y = [U\tilde{H}_E \quad \tilde{\alpha} U\tilde{H}_G]. \quad (67)$$

where we have approximated the scaling factor $\tilde{\alpha}$ by

$$\tilde{\alpha} = \frac{\|\tilde{G}_m\|}{\|\tilde{E}_m\|}. \quad (68)$$

Table 3 shows the error in approximation of Koopman frequencies and eigenvalues by the Exact Hankel-DMD method. The accuracy of computation is comparable to the single-observable Hankel-DMD method in section 3.1, however, since we are supplementing the observation on E with new measurements on G , we are able to capture new eigenfunctions, three of which are shown in the bottom row of figure 7.

6 Conclusion

In this paper, we have studied the convergence of DMD algorithms for ergodic systems. We introduced the Hankel-DMD method which can be used to compute the eigenvalues and eigenfunctions of the Koopman operator given the measurements on a single observable. We extended this methodology to the case of multiple observables using the Exact DMD algorithm. Our approach is based on approximation of the function projections using the vector projection in DMD, which is made possible by the Birkhoff's ergodic theorem. Using these methods, we were able to compute the Koopman spectrum using observations on a small number of observables in high-dimensional systems. We also showed the precise connection between SVD, which is frequently used in the DMD algorithms, and POD of ensemble of observables on the state space, and used it to represent chaotic dynamics on mixing attractors.

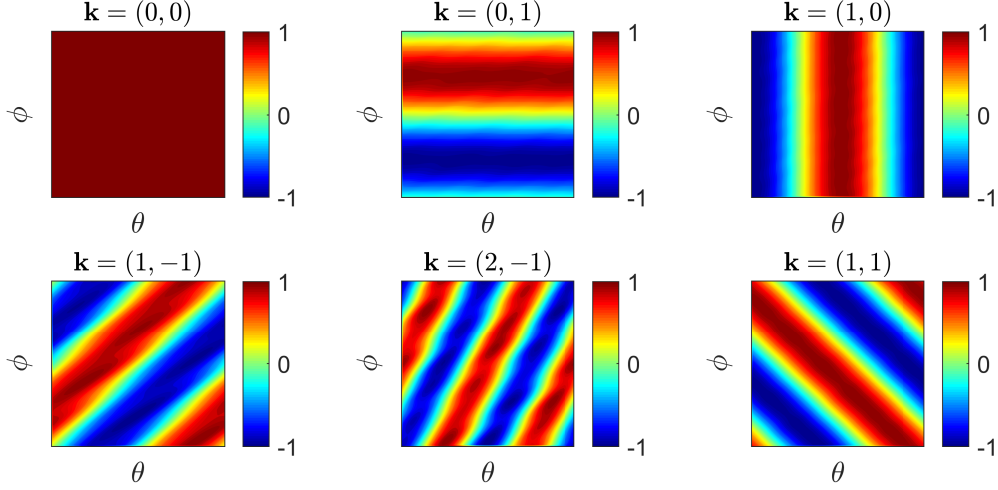


Figure 7: Real part of Koopman eigenfunctions $\tilde{\phi}_{\mathbf{k}}$ on the parameterized torus of quasi-periodic cavity flow at $Re = 16000$, computed using Exact Hankel-DMD.

k	$\tilde{\omega}^k$	ω^k ([26])	relative error	$var(\tilde{\phi}_k - \phi_k)$
(0,0)	0	0	0	$6.48e-9$
(0,1)	0.60892	0.60890	$1.67e-5$	$2.33e-3$
(1,0)	0.97624	0.97624	$5.86e-6$	$1.03e-3$
(1,-1)	0.36732	0.36728	$1.13e-4$	$3.81e-4$
(2,-1)	1.34353	1.34352	$3.68e-6$	$1.22e-2$
(1,1)	1.58515	1.58520	$3.23e-5$	$3.26e-3$

Table 3: Accuracy of the dominant Koopman frequencies and eigenfunctions for quasi-periodic cavity flow computed using Exact Hankel-DMD method.

SUPPLEMENTAL MATERIAL

The time series data and MATLAB codes of the numerical examples can be found at <https://ucsb.box.com/v/KMDandERGODICITY>.

ACKNOWLEDGMENT

This research has been partially supported by the ARO grant W911NF-11-1-0511 and the ONR grant N00014-14-1-0633. H.A. is grateful to Dr. Ryan Mohr and Nithin Govindarajan for some helpful mathematical discussions and comments on the manuscript.

References

- [1] B. O. Koopman. Hamiltonian systems and transformation in Hilbert space. *Proceedings of the National Academy of Sciences of the United States of America*, 17(5):315, 1931.
- [2] B. O. Koopman and J. von Neumann. Dynamical systems of continuous spectra. *Proceedings of the National Academy of Sciences of the United States of America*, 18(3):255, 1932.

- [3] Igor Mezić and Andrzej Banaszuk. Comparison of systems with complex behavior. *Physica D: Nonlinear Phenomena*, 197(1):101–133, 2004.
- [4] Igor Mezić. Spectral properties of dynamical systems, model reduction and decompositions. *Nonlinear Dynamics*, 41(1-3):309–325, 2005.
- [5] C.W. Rowley, I. Mezić, S. Bagheri, P. Schlatter, and D.S. Henningson. Spectral analysis of nonlinear flows. *Journal of Fluid Mechanics*, 641(1):115–127, 2009.
- [6] Peter J Schmid. Dynamic mode decomposition of numerical and experimental data. *Journal of fluid mechanics*, 656:5–28, 2010.
- [7] Yoshihiko Susuki and Igor Mezić. Nonlinear koopman modes and coherency identification of coupled swing dynamics. *IEEE Transactions on Power Systems*, 26(4):1894–1904, 2011.
- [8] Michael Georgescu and Igor Mezić. Building energy modeling: A systematic approach to zoning and model reduction using koopman mode analysis. *Energy and buildings*, 86:794–802, 2015.
- [9] Bingni W Brunton, Lise A Johnson, Jeffrey G Ojemann, and J Nathan Kutz. Extracting spatial-temporal coherent patterns in large-scale neural recordings using dynamic mode decomposition. *Journal of neuroscience methods*, 258:1–15, 2016.
- [10] Igor Mezić. Analysis of fluid flows via spectral properties of the koopman operator. *Annual Review of Fluid Mechanics*, 45:357–378, 2013.
- [11] RK Singh and JS Manhas. *Composition operators on function spaces*. Number 179. North Holland, 1993.
- [12] Igor Mezić. On applications of the spectral theory of the koopman operator in dynamical systems and control theory. In *Decision and Control (CDC), 2015 IEEE 54th Annual Conference on*, pages 7034–7041. IEEE, 2015.
- [13] Alexandre Mauroy and Igor Mezić. Global stability analysis using the eigenfunctions of the koopman operator. 2014.
- [14] Jonathan H Tu, Clarence W Rowley, Dirk M Luchtenburg, Steven L Brunton, and J Nathan Kutz. On dynamic mode decomposition: theory and applications. *Journal of Computational Dynamics*, 1:391–421, 2014.
- [15] Matthew O Williams, Ioannis G Kevrekidis, and Clarence W Rowley. A data-driven approximation of the koopman operator: Extending dynamic mode decomposition. *Journal of Nonlinear Science*, 25(6):1307–1346, 2015.
- [16] Anders C Hansen. Infinite-dimensional numerical linear algebra: theory and applications. In *Proceedings of the Royal Society of London A: Mathematical, Physical and Engineering Sciences*, page rspa20090617. The Royal Society, 2010.
- [17] Joshua L Proctor, Steven L Brunton, and J Nathan Kutz. Dynamic mode decomposition with control. *SIAM Journal on Applied Dynamical Systems*, 15(1):142–161, 2016.
- [18] Lloyd N Trefethen and David Bau III. *Numerical linear algebra*, volume 50. Siam, 1997.

- [19] Kevin K Chen, Jonathan H Tu, and Clarence W Rowley. Variants of dynamic mode decomposition: boundary condition, koopman, and fourier analyses. *Journal of nonlinear science*, 22(6):887–915, 2012.
- [20] Steven L Brunton, Bingni W Brunton, Joshua L Proctor, Erika Kaiser, and J Nathan Kutz. Chaos as an intermittently forced linear system. *arXiv preprint arXiv:1608.05306*, 2016.
- [21] Dimitrios Giannakis. Data-driven spectral decomposition and forecasting of ergodic dynamical systems. *arXiv preprint arXiv:1507.02338*, 2015.
- [22] Yoshihiko Susuki and Igor Mezić. A prony approximation of koopman mode decomposition. In *2015 54th IEEE Conference on Decision and Control (CDC)*, pages 7022–7027. IEEE, 2015.
- [23] K. Petersen. *Ergodic Theory*. Cambridge University Press, Cambridge, 1995.
- [24] Igor Mezić and Fotis Sotiropoulos. Ergodic theory and experimental visualization of invariant sets in chaotically advected flows. *Physics of Fluids (1994-present)*, 14(7):2235–2243, 2002.
- [25] Ulrich Krengel and Antoine Brunel. *Ergodic theorems*, volume 59. Cambridge Univ Press, 1985.
- [26] H. Arbabi and Igor Mezić. Study of dynamics in lid-driven cavity flow using koopman mode decomposition. *preprint*, 2016.
- [27] Igor Mezic. Spectral expansion in dissipative dynamical systems and its consequences for state space geometry and dynamically evolving data. *preprint*, 2016.
- [28] David Ruelle. *Chaotic evolution and strange attractors*, volume 1. Cambridge University Press, 1989.
- [29] Alexandre Mauroy and Igor Mezić. On the use of fourier averages to compute the global isochrons of (quasi) periodic dynamics. *Chaos: An Interdisciplinary Journal of Nonlinear Science*, 22(3):033112, 2012.
- [30] Peter Van Overschee and BL De Moor. *Subspace identification for linear systems: TheoryImplementationApplications*. Springer Science & Business Media, 2012.
- [31] Philip Holmes, John L Lumley, Gal Berkooz, and Clarence Rowley. *Turbulence, coherent structures, dynamical systems and symmetry*. Cambridge university press, 2012.
- [32] Lawrence Sirovich. Turbulence and the dynamics of coherent structures part i: coherent structures. *Quarterly of applied mathematics*, 45(3):561–571, 1987.
- [33] Edward N Lorenz. Deterministic nonperiodic flow. *Journal of the atmospheric sciences*, 20(2):130–141, 1963.
- [34] Stefano Luzzatto, Ian Melbourne, and Frederic Paccaut. The lorenz attractor is mixing. *Communications in Mathematical Physics*, 260(2):393–401, 2005.
- [35] Steven L Brunton, Joshua L Proctor, and J Nathan Kutz. Sparse identification of nonlinear dynamics with control (sindyc). *arXiv preprint arXiv:1605.06682*, 2016.